Shock Tube and Ballistic Range Facilities at NASA Ames Research Center

Jay H. Grinstead, Michael C. Wilder, Daniel C. Reda, and Charles J. Cornelison
NASA Ames Research Center
Moffett Field, CA 94035 USA

Brett A. Cruden and David W. Bogdanoff
ELORET, Inc.
Moffett Field, CA 94035 USA

Jay.H.Grinstead@nasa.gov

ABSTRACT

The Electric Arc Shock Tube (EAST) facility and the Hypervelocity Free Flight Aerodynamic Facility (HFFAF) at NASA Ames Research Center are described. These facilities have been in operation since the 1960s and have supported many NASA missions and technology development initiatives. The facilities have world-unique capabilities that enable experimental studies of real-gas aerothermal, gas dynamic, and kinetic phenomena of atmospheric entry.

1.0 INTRODUCTION

Entry, descent, and landing systems enable a safe transition from orbital or superorbital velocities through a planetary atmosphere for landing and recovery. They are a critical enabling technology for human and robotic space exploration missions. An important and necessary component of an entry system is the spacecraft's thermal protection system (TPS). Mission objectives and risk profile define the overall requirements for the TPS. These requirements, in turn, are both further refined and fulfilled through a development and qualification program coordinated across a variety of disciplines, including high temperature gas physics and chemistry, aerodynamics, aerothermodynamics, materials science, and metrology.

Ground testing programs utilizing high enthalpy test facilities support the development of entry systems technologies. High enthalpy facilities of different types can simulate the aerothermal environment of atmospheric entry over a range of conditions. Validation of computational tools used for TPS design is the driving factor for investment in and use of these specialized facilities. Material thermal response models are developed and validated through arc jet tests. Phenomenological aspects of atmospheric entry — real-gas thermochemistry, shock radiation kinetics and transport, and transition to turbulence — are investigated and characterized in hypersonic wind tunnels, shock tubes, and free-flight ballistic ranges. Computational fluid dynamics (CFD) simulations that incorporate real-gas kinetic and transport models, coupled with material thermal response codes and appropriate boundary conditions, become powerful and sophisticated tools for the design of a vehicle's TPS. As no single high enthalpy ground test facility is capable of producing all relevant transatmospheric flight conditions with adequate fidelity, the critical differences and shortcomings must be understood when choosing a facility, designing a test, interpreting its results, and integrating the results into a flight vehicle design tool.

Report Documentation Page

Form Approved
OMB No. 0704-0188

1. REPORT DATE	2. REPORT TYPE	3. DATES COVERED
APR 2010	**N/A**	**-**

4. TITLE AND SUBTITLE	5a. CONTRACT NUMBER
Shock Tube and Ballistic Range Facilities at NASA Ames Research Center	5b. GRANT NUMBER
	5c. PROGRAM ELEMENT NUMBER
6. AUTHOR(S)	5d. PROJECT NUMBER
	5e. TASK NUMBER
	5f. WORK UNIT NUMBER
7. PERFORMING ORGANIZATION NAME(S) AND ADDRESS(ES) **NASA Ames Research Center Moffett Field, CA 94035 USA**	8. PERFORMING ORGANIZATION REPORT NUMBER
9. SPONSORING/MONITORING AGENCY NAME(S) AND ADDRESS(ES)	10. SPONSOR/MONITOR'S ACRONYM(S)
	11. SPONSOR/MONITOR'S REPORT NUMBER(S)

12. DISTRIBUTION/AVAILABILITY STATEMENT
Approved for public release, distribution unlimited

13. SUPPLEMENTARY NOTES
See also ADA569031. Aerothermodynamic Design, Review on Ground Testing and CFD (Conception aerothermodynamique, revue sur les essais au sol et dynamique des fluides informatisee).

14. ABSTRACT
The Electric Arc Shock Tube (EAST) facility and the Hypervelocity Free Flight Aerodynamic Facility (HFFAF) at NASA Ames Research Center are described. These facilities have been in operation since the 1960s and have supported many NASA missions and technology development initiatives. The facilities have world-unique capabilities that enable experimental studies of real-gas aerothermal, gas dynamic, and kinetic phenomena of atmospheric entry.

15. SUBJECT TERMS

16. SECURITY CLASSIFICATION OF:			17. LIMITATION OF ABSTRACT	18. NUMBER OF PAGES	19a. NAME OF RESPONSIBLE PERSON
a. REPORT	b. ABSTRACT	c. THIS PAGE			
unclassified	**unclassified**	**unclassified**	**SAR**	**24**	

Motivated by the critical needs for safe re-entry into Earth's atmosphere, NASA Ames invested heavily in developing test facilities for the study of hypersonics, aerothermodynamics, and thermal protection materials and systems. Much of this effort began in earnest in the 1950s, and growth continued through the 1960s and 1970s in support of NASA's human spaceflight and planetary exploration missions. Today, Ames operates one of the most comprehensive networks of high enthalpy test facilities in the world and continues to support NASA, other government agencies, and private commercial programs for entry systems research and technology development.

Using advanced experimental techniques, simulation, and innovative test planning strategies, researchers and engineers at NASA Ames have pursued an approach to ground testing that maximizes the utility of Ames' high enthalpy facilities. Pathfinding research in fundamental aspects of aerothermal phenomenology has utilized Ames' shock tube and ballistic range facilities. Shock radiation spectroscopy of several planetary atmospheres has been investigated in the Electric Arc Shock Tube (EAST) facility. Heat transfer, transition to turbulence, and shock radiation have been studied in the Hypervelocity Free Flight Aerodynamic Facility (HFFAF), an aeroballistic range. This paper describes the history, features, and operation of these unique facilities, as well as a summary of the past and current research conducted using them.

2.0 HIGH-ENTHALPY IMPULSE FACILITES AT AMES – A BRIEF HISTORY

The early space age presented new challenges for development of technologies needed to realize national ambitions for space exploration. Since the late 1940s, Ames has been at the forefront of research into hypervelocity flight, atmospheric entry phenomenology, and thermal protection systems. From the 1950s through the early 1970s, Ames developed several high-enthalpy impulse facilities to advance critical research initiatives in atmospheric entry aerodynamics and aerothermodynamics. During that era, high-enthalpy impulse facilities were just as much a fertile area of research as the phenomena these facilities were built to investigate. Some of the facilities were short-lived – built and operated as prototypes for larger facilities. Others have been decommissioned because of disuse. The facilities that remain are the only free-flight ballistic range and high enthalpy shock tube within NASA and have world-unique capabilities. The test methodologies, practices, and instrumentation currently in use have been built upon decades of experience supporting NASA and non-NASA research efforts. An abridged timeline of seminal events places today's capabilities in context.

2.1 Hypervelocity facilities

Following World War II, the Ames Aeronautical Laboratory of the National Advisory Committee for Aeronautics (NACA) had developed several continuous-flow supersonic wind tunnel facilities. The maximum Mach number achieved in the fastest of these late 1940s-era facilities was approximately 6.0. It had become apparent that reaching ever-higher hypersonic velocities with continuous-flow wind tunnel facilities had reached practical limits in terms of thermodynamics, materials, size, and cost. In addition, because of decreasing free stream densities, the desired Reynolds number similarity was inching further beyond reach as Mach number increased in these continuous facilities.

In 1946, H. Julian Allen, a pioneer in planetary entry physics research, first proposed the use of ballistics ranges as a means to reach higher velocities [1]. Small-scale flight models would be fired down the range and observed for aerodynamic and aerothermodynamic responses. Allen thought that even higher velocities and hypersonic Mach numbers could be achieved by firing a model upstream against a supersonic wind tunnel flow – without the dismaying decrease in Reynolds number at higher Mach numbers suffered with wind

tunnels alone. The Supersonic Free Flight (SSFF) facility [2] was Ames' first major counterflow facility, completed in 1949. Improvements in gun performance and launching techniques enabled Mach numbers over 10 to be realized at flight-relevant Reynolds numbers.

Although the SSFF facility was key to generating new and important data at hypersonic speeds, uncertainties about turbulence produced by the supersonic counterflow – and its effect on model dynamic stability – prompted the development of the Pressurized Ballistic Range (PBR). The PBR, which became operational in 1958, was designed to launch models at speeds up to 3.3 km/s (approximately Mach 10) into a quiescent test gas at pressures up to 10 atm [3]. The high pressures and launch speeds yielded high Reynolds numbers for the study of turbulent flow at hypersonic Mach numbers. The PBR was used for aerodynamics [4-6] and ablation [7] research until it was decommissioned in the 1990s.

An offshoot in the development of counterflow facilities at Ames was the Atmosphere Entry Simulator [8,9]. This unique facility became operational in 1960 following development of a prototype in 1956. The motivation was to replicate the progressive increase in density and decrease in velocity encountered by a vehicle entering a planetary atmosphere. An expanding, contoured nozzle produced an accelerating supersonic flow with a concomitant exponential decay in density. A two-stage light gas gun fired models upstream through the expanding nozzle flow. Control of reservoir pressure and launch velocity tailored experiments for entry profiles with coupled altitude and velocity variations.

While these facilities were able to reach hypersonic Mach numbers, they were unable to replicate orbital and superorbital entry velocities encountered by planetary probes and human-rated spacecraft returning from the moon. The objective was to reach speeds in excess of 15 km/s, or Mach 50. Such extreme conditions could not be met by a counterflow facility consisting of the highest performance light gas gun and a continuous flow hypersonic wind tunnel. Only through the use of a high-enthalpy, hypersonic shock tunnel in counterflow could the 15 km/s goal be approached. Ames scientists Alvin Seiff and Thomas Canning pursued development of this ultimate counterflow facility. The challenges of synchronizing the model launch and impulsive shock tunnel flow were formidable. A pilot facility was constructed in 1958 to prove the concept [10], followed by a prototype in 1961 [11].

The pilot facility not only established the viability of the shock tunnel counterflow concept, it also performed well as a research facility. Launch speeds of 3-8.8 km/s and a Mach 6 counterflow at 1.8 km/s reached combined speeds relevant to superorbital entry. Shock radiation measurements obtained over a range of speeds and densities revealed significant magnitude differences between equilibrium and nonequilibrium radiation [12]. Ablation of plastic models was also investigated [13]. The prototype facility, which was larger in all respects, utilized a combustion driver for the shock tunnel. Launch speeds were slightly higher than with the pilot facility, and the shock tunnel generated Mach 7 flows at velocities up to 3.7 km/s [14]. The facility was capable of combined speeds up to 12.5 km/s and supported research for aerodynamics [4,15], shock radiation [16-20], and heat transfer [21].

With successful demonstration of the ballistic range/shock tunnel configuration, approval and funding for the Ames Hypervelocity Free Flight (HFF) complex was obtained in 1963. The complex was completed by 1966 at a cost of $5M (roughly $40M in 2010 dollars). The HFF complex was composed of three facilities: the HFF Gun Development Facility (HFFGDF), HFF Radiation Facility (HFFRF), and the HFF Aerodynamic Facility (HFFAF) [22]. The radiation and aerodynamic facilities were designed for counterflow operation generated by combustion-driven reflected shock tunnels. Both were used for studies of radiation, ablation, and effects of ablation-induced shape change on vehicle aerodynamics. The HFFGDF was devoted to improvement of light gas gun launchers.

The facilities of the HFF complex were used for investigations of the Apollo command module aerodynamics at lunar return conditions [23]. By the end of the Apollo program, however, NASA's direction largely shifted away from exploration objectives for which the full capability of the HFF complex was originally designed. The last of the counterflow experiments was in 1972. That same year the HFFRF was decommissioned. The space occupied by the HFFGDF was claimed for other projects in the 1990s. The HFFRF was reactivated in the early 1990s [24] and later repurposed as a new HFFGDF in 1997. The HFFAF remained in operation but without utilizing its counterflow capability. In the 1970s and 1980s, its ballistic range supported entry system aerodynamics research for flight missions: Mars Viking [25], Pioneer Venus [26], Galileo (Jupiter) [5], and PAET (Planetary Atmosphere Experiments Test, an Earth entry vehicle) [27]. The shock tunnel of the HFFAF was reactivated and operated for several years in the early 1990s to support scramjet propulsion research for the National AeroSpace Plane (NASP) program [28]. The ballistic range of the HFFAF was refurbished in the late 1990s after decades of service. Subsequent aerodynamics research was dedicated to technology demonstrators and future flight vehicles such as the entry capsule for the Mars Science Laboratory (MSL) [29] and Crew Exploration Vehicle command module (CEV/Orion) [30]. Today, in its fifth decade of service, the HFFAF supports basic research in boundary layer transition due to surface roughness [31-33].

2.2 Shock tube facilities

The ability to replicate the gas dynamic conditions in the shock layer ahead of vehicles travelling at very high speeds would enable the study of important kinetic and radiative phenomena. The need for experimental data was compelling – theoretical analyses indicated that dissociation, ionization, and radiation play a significant role in defining the state of shock-heated gases at conditions considered for atmospheric entry into Earth and other planetary atmospheres. Radiative heating can surpass and dominate over convective heating as vehicle speeds and sizes increase. The chemical kinetic mechanisms, emitted spectra, and radiation transport at these extreme conditions were largely unknown in the 1960s. As with other emerging fields of aerospace physics, ground test validation of simulations was critical for system studies and vehicle design. Concurrent with shock radiation research in the hypervelocity facilities, Ames also pursued the use of shock tubes for kinetics and radiation studies, as well as for development and maturation of ground test capabilities.

A small number of shock tube and shock tunnel facilities were built in the 1950s and 1960s. Some were built specifically for use with the hypervelocity free flight facilities. Apart from that application, other shock tubes and tunnels were built and operated in the 1960s as dedicated research facilities. A combustion-driven shock tunnel with a 30.5 cm square test section was built in 1962 [34]. The operating characteristics of this driver were studied for the development of the two larger shock tunnels of the HFF complex. Efforts were also directed towards improving facility performance by examining driver combustion [35] and diaphragm rupture [36]. A smaller, 16.8 cm dia. combustion-driven shock tube was used extensively in the late 1960s and early 1970s for a variety of kinetics and radiation studies of CN [37-40], C_2 [41], and N_2^+ [40].

Limitations on shock speeds produced by combustion drivers prompted the development of the first electric arc-driven shock tubes at the General Electric Space Sciences Laboratory [42,43] and the AVCO-Everett Research Laboratory [44,45] in the early 1960s. The first arc-driven shock tube at Ames was built shortly thereafter [46]. The Ames facility had a 13.96 cm dia. driver and 30.47 cm dia. driven tube. The 1 MJ capacitor bank was operated at a maximum voltage of 20 kV. The design maximum shock speed was 12 km/s. The facility was used for N_2 shock radiation measurements in the vacuum ultraviolet [47], dissociation kinetics of CO in CO_2-bearing atmospheres [48], and precursor ionization ahead of shock waves in air and nitrogen [49].

The Electric Arc Shock Tube (EAST) facility was built in 1965 under contract from General Electric and was patterned after one of their later arc-driven facilities. It is comprised of an arc driver, a 10.16 cm dia. shock tube, and a 76.2 cm exit diameter nozzle for reflected shock tunnel operation [50]. Its 1 MJ capacitor bank is rated to 40 kV. The primary purpose of the facility when designed and built was for use as a high enthalpy shock tunnel.

The EAST facility has been used for the study of vibrational and rotational relaxation in expanding nitrogen flows [51,52], demonstration of a magnetohydrodynamic accelerator [53], carbon nitridation [54] and the measurement of the electrical conductivity of shock heated air [55]. The EAST was also used to examine substitution of N_2O/N_2 mixtures as the working fluid for shock tunnels as a means to increase testing time [56]. In the late 1970s, radiative base heating of the Galileo probe to Jupiter was explored [57]. An early reported application of the EAST facility was the examination of hydrometeor interaction with shock waves [58], a phenomena encountered by ballistic missile entry through clouds and droplets.

Besides applied research efforts, a significant effort was devoted towards characterizing and improving the performance of the EAST facility – and arc-heated shock tubes and shock tunnels in general [59-61]. Most of this development work was conducted from the late 1960s through the early 1980s.

Currently, the EAST is dedicated to shock radiation spectroscopy for Earth and planetary entry radiative heating – still an important area of research after almost fifty years. Recent published results report spectroscopic measurements and analyses for lunar return to Earth [62,63] and aerocapture for Mars [64] and Titan [65] atmospheres. Earlier work in the 1990s examined shock radiation in air and nitrogen [66,67] and line shape analysis of atomic oxygen in the vacuum ultraviolet [68]. The interaction with radiation emitted by the arc driver and the driven gas prior to shock arrival has been investigated [69]; absorption of radiation from the He or H_2 driver gas with a He/H_2 mixture simulating gas giant atmospheres can have significant implications for shock radiation studies.

The EAST facility is the only shock tube in use at NASA Ames. The test methodologies and instrumentation developed over the last several years have significantly enhanced the capabilities of the facility. The following section describes the EAST as it exists today.

3.0 ELECTRIC ARC SHOCK TUBE (EAST) FACILITY

The EAST facility was intended to produce shock-heated gas environments at very high enthalpies. The facility design was informed by the known driver technologies and their limitations. The highest primary shock speeds in a shock tube are generated using a driver gas with a high speed of sound and a small ratio of specific heats. The four widely-used types of drivers for hypersonic facilities are:

- Heated light gas (He or H_2)
- Combustion or detonation of H_2, O_2, and He mixtures
- Adiabatic compression of He or He/Ar mixtures (free-piston driver)
- Arc discharge

Heated light gas drivers use electric heaters and are limited to approximately 700 K. Combustion and detonation drivers are limited to the adiabatic combustion temperature of the mixture. Even higher temperatures are possible with a piston driver, but the brief duration that the driver gas is held at high temperature and pressure can still be sufficient to compromise the structural integrity of the driver's materials.

The arc discharge driver can generate extreme temperatures above 10,000 K for much less than one millisecond, resulting in the highest shock speeds of the four driver types.

It needs to be noted that there are means of producing shock speeds that exceed the primary shock speeds obtainable from the first three driver types discussed above. Expansion tube facilities increase the kinetic energy of the shock tube test gas through unsteady expansion waves generated by shock propagation through a second accelerating gas. The speed of the shock travelling through the accelerating gas exceeds that obtainable as a primary shock, and the expansion tube has been adapted as a means to generate high shock speeds with light gas [70], detonation [71], and free-piston [72,73] driver types. Shock velocities up to 10-14 km/s can be produced using the expansion tube technique. With potential research for Jovian entry aerothermodynamics as a facility capability requirement, the arc driver was selected as being the only viable driver technology capable of reaching the required shock velocities of up to 46 km/s.

3.1 Facility configuration and operation

Many elements of the EAST facility have been upgraded or refurbished in the years since it first came into service, though the basic operating principles [74] of the facility are unchanged. A schematic of the EAST facility is shown in Fig. 1. The major components are the arc driver, driven tube, test section, dump tank, and vacuum system. A year-long upgrade of the facility was completed in 2008 in which a new test section, vacuum and gas loading system, data acquisition system, and spectroscopic instrumentation were installed.

3.1.1 Arc driver and power system

Since the beginning of EAST operations in 1965, the arc driver section has consisted of a variety of components assembled in several configurations. The initial driver designs were cylindrical with lengths of 137 cm and 290 cm. The later version was shortened to 76 cm. The ultimate pressure in these cylindrical drivers was reached near the end of the arc discharge. The metal diaphragm thicknesses were chosen to burst at one-half to one-third of the expected ultimate pressure [74]. Shock velocities of 16 km/s had been achieved with cylindrical drivers, but still higher velocities were sought. Increases in shock speed would require even higher temperatures (and pressures) in the driver, but operational limitations precluded possible improvements with cylindrical drivers. In 1971, Menard [75] demonstrated a novel new approach with the short, small-volume conical driver. The conical driver operates in a much different manner than the cylindrical driver. A thin Mylar or aluminium diaphragm begins to disintegrate shortly after onset of the discharge. Heating of the driver gas within the chamber continues as the gas expands into the driven tube. The comparatively small volume of the conical driver results in energy densities nearly

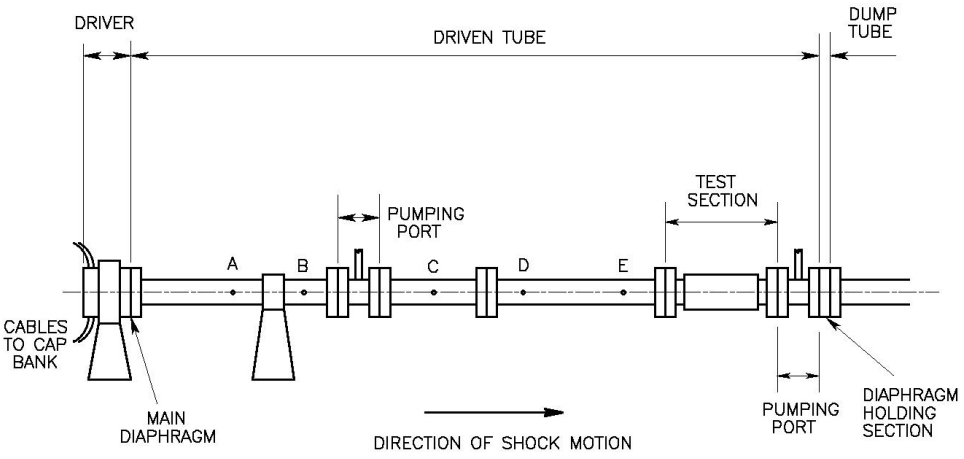

Figure 1: Schematic of EAST facility.

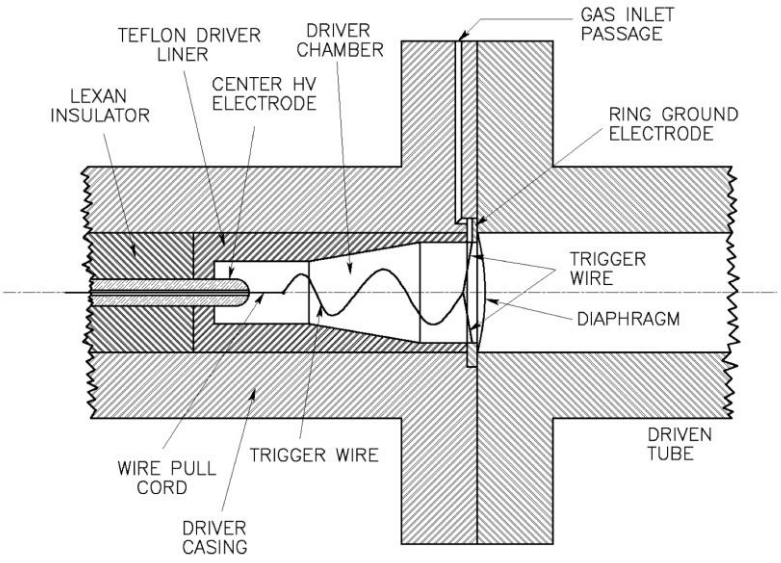

Figure 2: Electric arc driver.

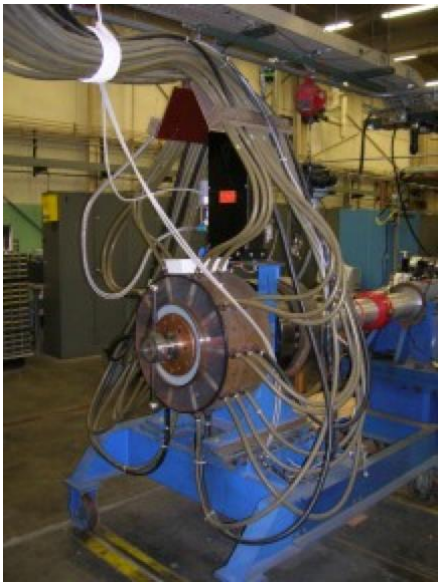

Figure 3: Collector ring assembly.

five times greater than with the cylindrical driver using the same energy source. The ultimate pressure achieved in the conical driver could be expected to be larger than with the cylindrical driver. Shock speeds of 46 km/s have been achieved with the conical driver [76]. Although the conical driver is used for most applications, the cylindrical driver is preferred for shock velocities below 8 km/s at driven tube pressures above 1.3 kPa (10 torr) [74]. The required shock velocity is the most important parameter in choosing between the conical and cylindrical drivers.

The current version of the conical driver is shown in Fig. 2. A Teflon liner forms the conical shape of the driver chamber. The aluminium (or, occasionally, Mylar) diaphragm is installed at the large end of the chamber, encircled by a ring ground electrode. The high voltage electrode is inserted into the center of the narrow end of the chamber. The driver chamber is 25.6 cm long and has a volume of 1292 cm^3. The chamber has two cylindrical sections with diameters of 6.35 and 10.16 cm joined by a conical tapering section. The high voltage electrode is connected to a current collector ring. One end of the tungsten trigger wire is attached to the ring ground electrode. The other end of the wire is tied to a non-conducting pull cord. The cord passes through a narrow hole in the center of the high voltage electrode. The end of the cord connects to the piston of a pneumatic solenoid. Once the high voltage set-point of the capacitor bank (see below) is reached, the piston withdraws the cord and trigger wire towards the high-voltage pin, completing the circuit and initiating the discharge. The collector ring and driver electrode assembly, shown in Fig. 3, consists of two coaxial copper cylinders. The outer cylinder is flanged to the driver and is electrically grounded. The inner cylinder is connected to the main electrode by a copper spring contact plate.

The power system at the Ames EAST facility consists of three main components:

- 40 kV constant current DC power supply
- 1.2 MJ 20/40kV DC fused capacitor storage system
- 40 kV-rated collector/driver electrode assembly

Figure 4: 1.2 MJ capacitor bank.

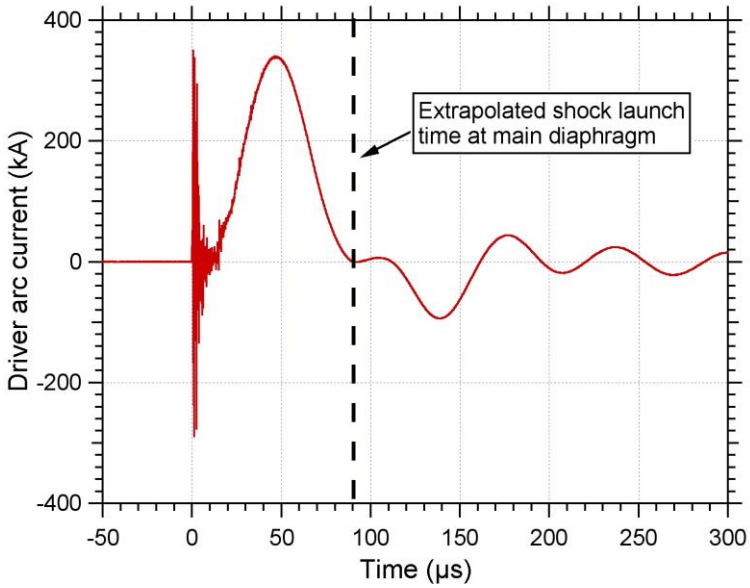

Figure 5: Arc current transient.

The capacitor storage system shown in Fig. 4 is a six-tier capacitor bank containing 220 capacitors. By using different combinations of series-parallel connections, the capacitance of the bank can be varied from 149 μF to its maximum value of 6126 μF (1530 μF for 40 kV operation). Nominal total system inductance, exclusive of the load (arc) is 0.26 μH, and the resistance is 1.6 mΩ. RG-17 coaxial cabling connects the capacitor bank to the collector/driver electrode assembly, and the entire system is regulated by a control system that includes discharge and shorting equipment, relays, control and permissive systems.

Figure 5 shows a graph of a typical driver current history. The peak current of 340 kA was reached at approximately 49 μs after discharge initiation. The capacitor bank energy for this run was 73 kJ and the estimated maximum power applied to the driver gas was 1.8 GW. From the shock wave position vs. time line (world line) recorded by the time of arrival sensors along the driven tube (Section 3.1.7), the launch time of the shock (at the main diaphragm) was extrapolated back to be approximately 40 μs after the current peak. This is a representative time delay for these EAST operating conditions. For Mylar diaphragms 0.036-0.050 cm thick, the time to fully open the diaphragm was estimated to be 20-40 μsec [76]. For the run for the data shown in Fig. 5, the diaphragm was 0.031 cm thick. The aluminium diaphragm is 15-65% heavier than the Mylar diaphragms, and this, coupled with the lower driver energy for the present case, would be expected to cause the diaphragm to open more slowly. Thus, the observed times between the current peak and the shock launch seem to be reasonably consistent with the estimated times to open the main diaphragm.

3.1.2 Driven tube

The driven tube currently installed in the EAST facility consists of a 6061 aluminum tube. The inner diameter is 10.16 cm. The outer diameter is 17.78 cm. The length from the main diaphragm to the downstream diaphragm is 9 m. As shown in Fig. 1, there are two pumping ports located at either end of the driven tube. The upstream pumping port is located near the main diaphragm. The downstream port is located after the test section, ahead of the downstream diaphragm.

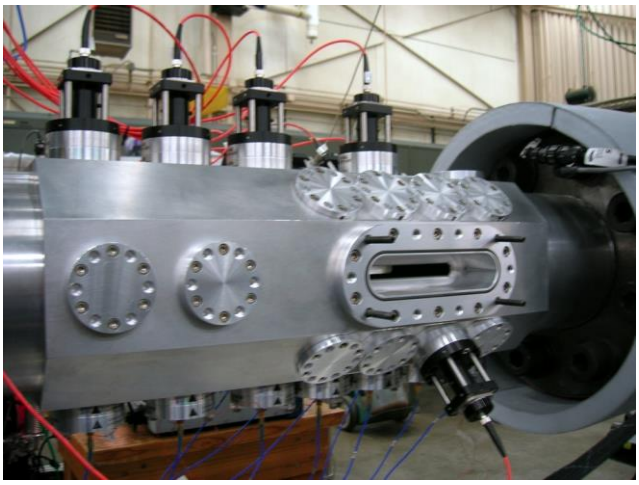

Figure 6: EAST test section.

A 61 cm diameter stainless steel driven tube was introduced in 1974. The arc driver can be moved to operate with either driven tube. The larger diameter enables operation at lower driven tube pressures because of the diminished influence of boundary layer growth [77]. Though currently available, the last use of the 61 cm driven tube was in the mid 1980s.

3.1.3 Test section

A new test section for shock radiation measurements was installed in late 2008. It expands the data collection capabilities of the EAST facility and also includes design features to improve operation. The test section, shown in Fig. 6, has two 12.1 cm long slot windows for imaging spectroscopy. It also has 32 round ports for time-of-arrival (TOA) sensors and for future expansion. The round ports are located such that up to 11 different axial positions may be monitored on the test section, with 7 additional positions upstream. Both the round and slot window ports were designed to reduce the recess between the inner surface of the window and tube wall by using tapered windows. A two-part (primary and secondary) assembly enables the window's vacuum seal to be moved away from the window's inner surface. The primary, which encapsulates the secondary, is inserted into the tube and provides a seating face for the window or pressure sensor. The secondary supports the window, provides the vacuum sealing surface, and also retains the window when removed from the primary. The rectangular slot windows use this same design concept, but with an elongated shape. An assembly drawing of a typical round window port is shown in Fig. 7.

3.1.4 Dump tube and dump tank

The dump tube is similar in construction to the driven tube and is 7 m long. A thin aluminium foil diaphragm separates the driven tube proper from the dump tube. The downstream end of the dump tube is attached to a steel holding (dump) tank. The dump tank is held at a moderate vacuum, approximately 2 Pa. When the shock bursts the downstream diaphragm, pressure differentials between the driven tube and the dump tube/tank system allows the gases to move into the dump tube and be held in the dump tank.

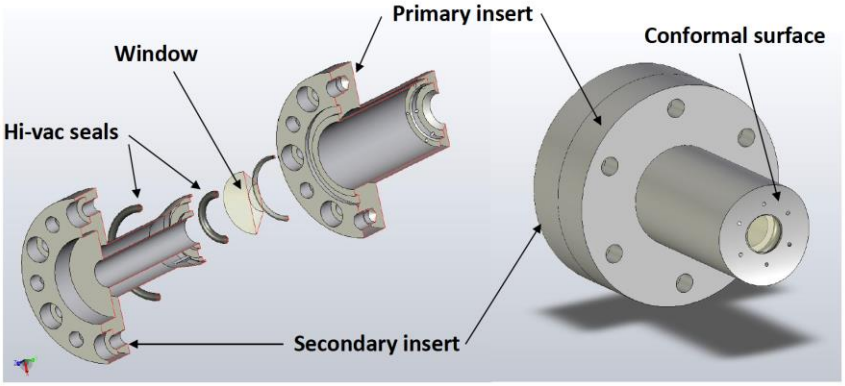

Figure 7: Test section window port. Inside surface of window is tangent to tube wall.

3.1.5 Vacuum and gas loading systems

The vacuum system for the EAST driven tube includes the two pumping ports, their vacuum pumps, several pressure gages, and a heater blanket. The

pumping ports have poppet valves that, when closed, conform to the inner surface of the shock tube wall. Turbomolecular high-vacuum and oil-free mechanical backing pumps are attached to each port valve housing. The pressure gauges on the driven tube are monitored by a dedicated data acquisition system which tracks and stores the pumpdown and pressure history of the vacuum system over extended periods of time. This system can also be used to diagnose vacuum system failures. A programmable logic controller (PLC) executes an automated overnight pumping procedure. The PLC operates the valves and heater blanket. The procedure engages alternating pump/purge and heat cycles to improve the ultimate vacuum base pressure in the driven tube by promoting H_2O and CO_2 desorption. A control panel built to interface with the PLC also provides a convenient central station for the shock tube operator to control all the valves in the facility. The driven tube reaches a base pressure of approximately 0.7 mPa ($5x10^{-6}$ torr) after a 12 hour pumping cycle.

A cold oxygen plasma source has been introduced to improve vacuum performance and remove carbon contaminants. This system uses radiofrequency (RF) power to create an oxygen plasma in a tube connected to the side of the driven tube upstream of the test section. Oxygen radicals produced within the cleaning unit enter the driven tube and travel in either direction from the entry port, reacting with carbon and other non-volatile species on the wall of the tube. The oxygen radicals are long-lived, and their presence is identified by a whitish-green glow (metastable O auroral line at 558 nm) in the tube. At a pressure of 0.27–0.67 Pa (2-5 mtorr), the plasma can be seen to extend as far as 1.5 m in either direction from the source, which is approximately 1.7 m upstream of the test section. The plasma source cleans a 3 m length of the driven tube, including the slot windows used for the imaging spectrograph instrumentation. Residual gas monitoring of the tube during cleaning shows an increase in peaks at molar masses of 44 and 84 g/mol, attributed to CO_2 and $CF_2(OH)_2$, respectively. The latter originates from vaporized products of the Teflon driver liner. Following a cleaning cycle, new mass peaks are observed at masses 47, 51 and 66 that are attributed to oxidized hydrofluorocarbon byproducts. The oxygen cleaner is operated between shots during the overnight pump/purge cycle for approximately 13 hours. Combining the oxygen plasma cleaning with heat and purge cycles is more successful in sweeping these byproducts out of the tube.

An automated gas loading system for the driver gas was developed and implemented as part of the 2008 modifications. The system brings the tube to a desired pressure set point in less than one minute. It has been interfaced with the shock tube firing controls. The procedure to fill the driven tube with the test gas is initiated at the same time as the capacitor bank charging sequence. The pressure in the tube is typically within 1-2% of the programmed set point before the driver fires.

3.1.6 Data system

The data acquisition system for the facility instrumentation utilizes two types of transient digitizer cards – five high-speed (200 MS/s) 4-channel cards from ZTEC Instruments, and three low-speed (5 MS/s) 8-channel cards from Spectral Dynamics. All digitizers have 16-bit resolution, and digitization error is below the instrument noise levels. Presently, the high-speed cards are connected to piezoelectric pressure TOA sensors and the low speed cards are connected to photomultiplier tube (PMT) TOA sensors upstream of the test section. Digitizer channels are also assigned to record current and voltage from the arc driver and the array detector pulse triggers. The arc current transient is used to trigger the data acquisition system.

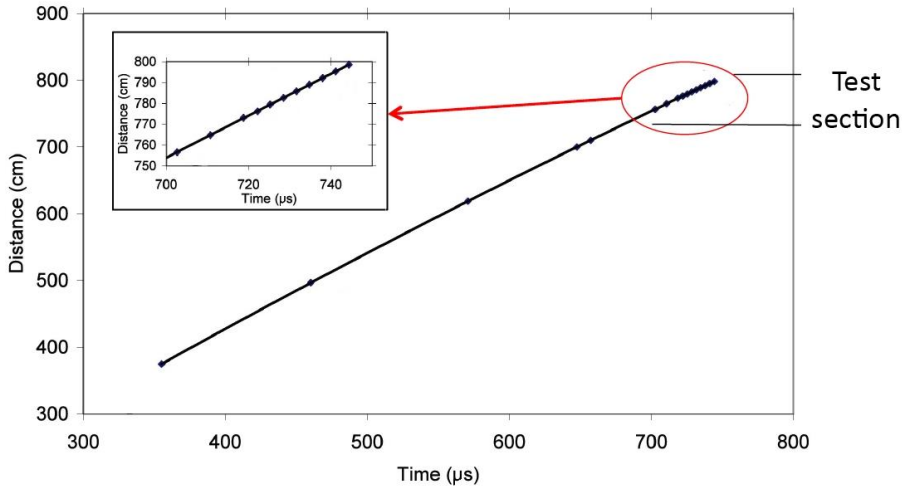

Figure 8: World lines (shock location vs. time) used to determine shock velocities. The inset shows the region of the test section.

3.1.7 Facility monitoring instrumentation

Photomultiplier tubes (PMTs) and piezoelectric pressure sensors are used as TOA sensors at several locations along the driven tube. The arrival times and their locations are used to compute shock velocities. The PMTs respond to the light emitted by shock-heated gas, while the pressure transducers respond to the pressure jump across the shock. The miniaturized PMTs have been mounted on a 48.3 cm (19") panel. Each panel contains 7 PMTs that are controlled by a single power source and control voltage. The PMTs are coupled to the round test section window ports via fiber optic cables. Between the fiber end and the window port are two slits approximately 20 cm apart. The slits are oriented and aligned normal to the shock tube axis. The light emitted by the shock is apertured to define a thin spatial region in order to optimize the temporal resolution of the shock arrival time. Output signals from the PMTs are fed through coaxial connectors that are, in turn, connected to the transient data system. Up to 18 pressure sensors and 16 PMTs may be installed on the system for time of arrival sensing. Additional PMTs are installed for use as triggers for the imaging spectrograph cameras; these PMTs use higher gain settings than the TOA PMTs to ensure reliability of the trigger.

Following the 2008 modifications, the velocity measurement capability was improved with the use of 18 different TOA ports, 9 of which are located directly around the imaging spectrograph window – the critical location where the greatest possible accuracy is needed. Prior to the modifications, the number of sensors was fewer and separated by longer distances. The achievable accuracy is illustrated in Fig. 8, which plots shock world line in both the pre-2008 and current EAST configurations. Both shocks have nominal velocities of 10.0 km/s but are slightly offset in distance and time because of the lengthening of the shock tube and changes to the trigger system following the modifications. The standard error of regression on the two data sets shown here is about 0.6%, though this number varies 0.4% to 1.0% from shot to shot. The error is smaller for the new TOA data because of the increased number of points (higher density of TOA gauges). More rigorous statistical analysis methods indicate that the standard error in velocity measurement is now 0.1-0.4%. This error however is smaller than the deceleration of the shock as it transits the rectangular window, so indicates a practical lower bound on shock speed accuracy.

3.2 EAST performance envelope and operating characteristics

The EAST facility has been run over 1000 times since 1965. Data from the years of use enable compilation of a record of test conditions and configurations. Figure 9 shows the envelope of achievable test conditions. Since the impedance of light gases is less than that for heavier gases, the shock velocities in light gases are appreciably higher for the same facility operating parameters. Two boundaries are shown. The air boundary

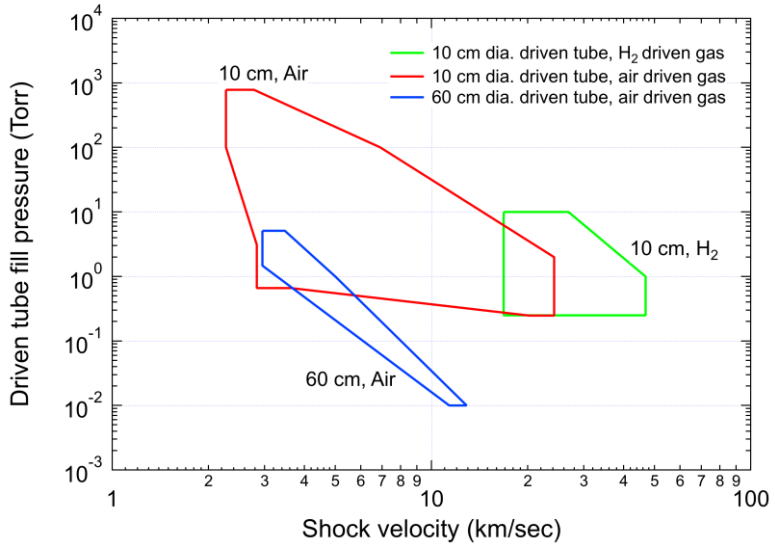

Figure 9: EAST operating envelopes.

represents the atmospheres of Earth, Mars, Venus, Titan, and pure molecular gases such as nitrogen. The H_2 boundary represents H_2/He gas giant atmospheres. The record also informs selection of facility parameters (primarily voltage) for realizing new pressure/velocity test points.

The definitive references on the operation of the EAST facility are two papers covering the driver and driven tube, respectively, by Sharma and Park [76], and an operations report by Dannenberg [74]. These references discuss performance envelopes (as of 1990), arc driver chemistry and electrical modelling of the driver circuit, correlation of operating parameters with shock velocity, and comparisons between measured and computed shock velocities as a function of operating parameters.

The test time of a shock tube is defined by the interval between passage of the shock and arrival of the contact surface (the interface between shocked driven gas and driver gas). Arc-driven shock tubes exhibit shorter test times with higher variability than shock tubes with other driver types. For shock radiation studies, desirable test times are sufficiently long if the initial, post-shock nonequilibrium overshoot relaxes to equilibrium prior to arrival of the driver gas. Fig. 10, reproduced from ref. [76] shows the test times achieved behind the incident shock achieved in the 10.16 cm driven tube with the conical driver. These test times range from 1 to 20 μsec. The general trend is that test time decreases at higher velocities and lower driven tube pressures.

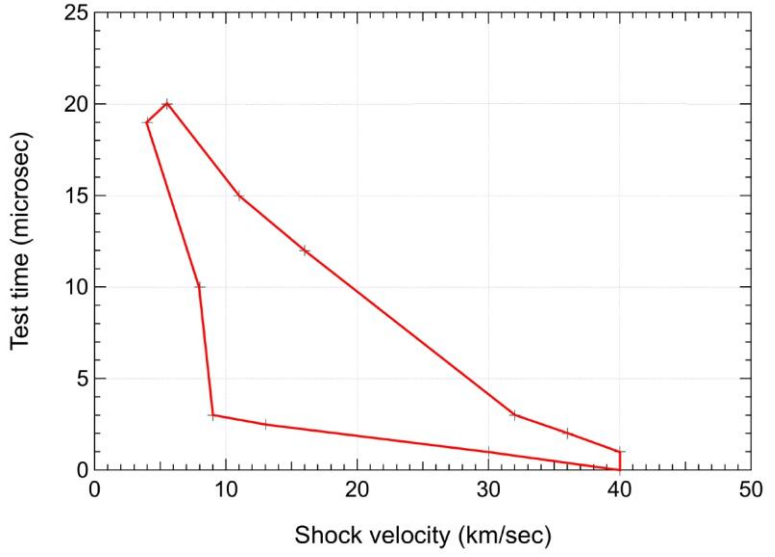

Figure 10: Envelope of observed test times vs. shock velocity.

Much longer test times have been achieved at lower shock velocities using the 76 cm dia. cylindrical driver with air and N_2O/N_2 mixtures as the test gases [56]. At pressures of 8-90 kPa and shock velocities of 2.1-3.0 km/sec, test times of 80-420 μs were obtained. The shortest test times were at the highest shock velocities with air as the driven tube gas, and the longest test times were at the lowest shock velocities and with N_2O/N_2 as the driven tube gas.

Buffer sections interposed between the main diaphragm and test gas have been investigated as a means to increase test

time. The buffer, which is typically filled with a gas 10 to 1000 times as dense as the driven gas, is intended to act as a heavy gas piston and to hold back jets of the driver gas from penetrating into the driven gas. Increases in test times with buffers using the 76 cm dia. cylindrical driver have been observed. For 53% N_2O/balance N_2 driven gas mixtures at shock velocities of 4 to 6 km/sec, the best buffers were found to increase the test time by factors of 1.5 to 3.0. The largest increases in test time were observed at the lower shock velocities.

The use of a buffer was also attempted for use at very high shock velocities in H_2/He simulating gas giant atmospheres. The driven gas was at 133 Pa (1 torr) pressure and the buffer gas was at 1.33 kPa (10 torr) pressure. At these very high shock velocities, the introduction of the mass of the buffer and the buffer diaphragm were found to produce substantial losses (6-10 km/sec) in shock velocity. For this reason, the buffer concept was abandoned for these very high shock velocity test conditions. Research on the use of buffers is ongoing.

4.0 HYPERVELOCITY FREE FLIGHT AERODYNAMIC FACILITY (HFFAF)

As discussed in Section 2, the HFFAF is NASA's only aeroballistic range facility and occupies a unique position in its capability to support aerodynamic and aerothermodynamic testing for basic and applied research. The details of the major facility components, including the shock tunnel, are described in detail in this section.

4.1 Facility configuration

The HFFAF consists of a model launching gun (light gas or powder), a sabot separation tank, a test section with 16 orthogonal shadowgraph imaging stations, an impact/test chamber, and the combustion-driven shock

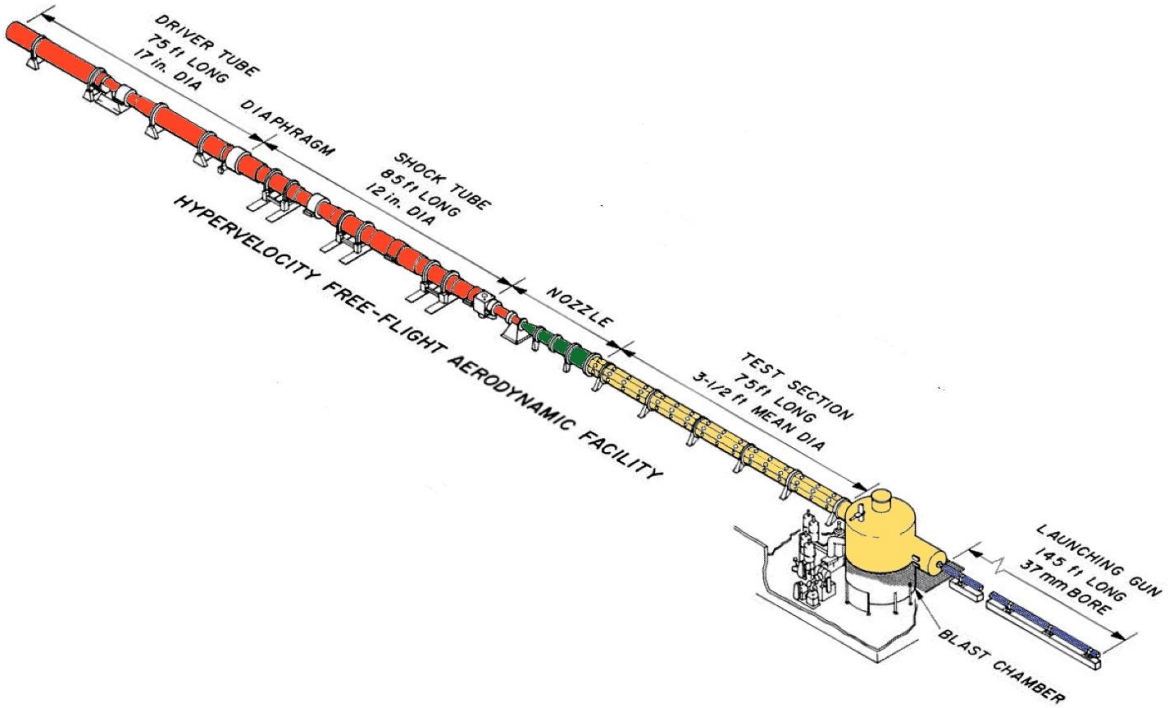

Figure 11: Hypervelocity Free Flight Aerodynamic Facility (HFFAF).

Table 1: Launch guns for HFFAF.

Gun type	Launch tube dia. (mm)	Muzzle velocity (km/s)	Sabot-launched projectile dia. (mm)	Launch mass (g)
Light gas	7.1, 12.7, 25.4, 38.3	1.8 – 8.5	1.6 – 31	0.2 – 400
Powder	20, 25, 44, 61	0.2 – 2.4	3.2 – 51	0.5 – 200
Air	25.4	0.2 – 0.5	6.4 – 20	2 – 20

tunnel. An overview schematic of the HFFAF is shown in Fig. 11. End-to-end, the facility measures over 125 m. The facility is on ground level, and the control room is located one floor below.

4.1.1 Launchers

Light gas, powder, and air gun launchers are used with the HFFAF. Table 1 lists the guns and their specifications. A two-stage light-gas gun typically consists of a powder chamber, pump tube, high-pressure coupling, and launch tube (Fig. 12). A deformable plastic piston is inserted into the upstream end of the pump tube. The sabot (which holds the model) is inserted into the launch tube breech, and a burst disk (diaphragm) is placed between the high-pressure coupling and launch tube. The sabot is made of two or four interlocking fingers that separate after the launch package exits the muzzle, releasing the model. The pump tube is evacuated and filled with a predetermined amount of hydrogen, and a gunpowder charge is placed in the powder chamber. Igniting the gunpowder charge fires the facility. The expanding gunpowder gases accelerate the piston, compressing the H_2 in the pump tube, or first stage, of the gun. At a predetermined pressure, the burst disk ruptures, and the compressed H_2 released from the pump tube acts upon the base of the sabot. The expanding H_2 accelerates the launch package down the launch tube, or second stage, of the gun. When the sabot and model exit the launch tube, they enter the separation tank where the sabot is stripped away from the model by aerodynamic forces or by muzzle gas blast acting on a hole in the base of the sabot. The model passes through a small aperture and enters the test section, leaving the separated sabot behind.

A powder gun is a simpler design and consists of a powder chamber and a launch tube. The launch package (sabot and model) is loaded into the launch tube breech, and a gunpowder charge is placed in the powder chamber. As with the light gas gun, igniting the gunpowder charge fires the facility. The expanding gases accelerate the launch package (sabot and model) down the launch tube and into the separation tank. The sabot is stripped away, and the model continues through to enter the test section in the same manner as models launched with the light gas gun. An air gun relies only on a reservoir of compressed air to launch models at velocities of 0.2 to 0.5 km/s.

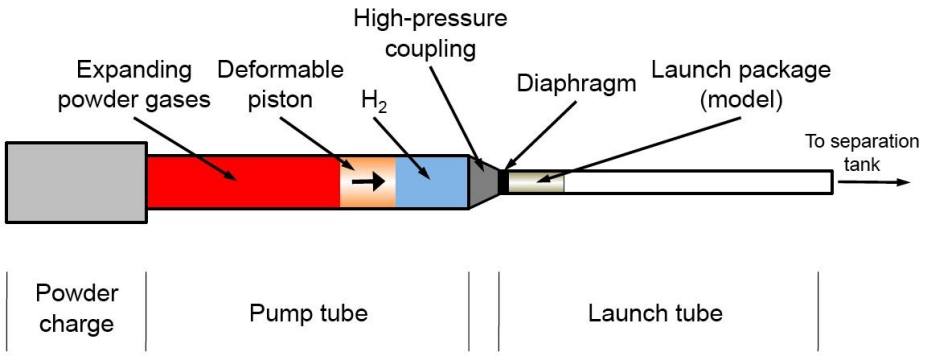

Figure 12: Schematic of two-stage light gas gun.

The performance of the light gas guns depends upon many, and sometimes conflicting, variables such as pump tube pressure, piston weight, gunpowder charge, burst disk (diaphragm) pressure rating, and launch package weight. A realistic maximum launch velocity is 8.5 km/s for robust models such as spheres and cylinders. For delicate

aeroballistic models, maximum velocities are typically limited to 4.5-6.5 km/s. Sabot-launched model diameters typically vary between 15 to 80% of the gun barrel diameter. Similarly, model masses typically vary from 0.2 to 200 grams. The lower limit velocity for each of the light gas guns is approximately 1.8 km/s. A detailed description of light gas guns and their operating characteristics can be found in reference [78].

Successful ballistic range experiments in large measure rely on the design of ballistic range models and sabots. Launch packages must tolerate very high launch acceleration loads. Aerodynamic forces are negligible by comparison. The sabot pieces must separate from the model without imparting angular displacement or velocity perturbations.

Some models are designed as bore riders and have no sabot. The launch package placed in the launch tube is the model itself. Bore rider models are axisymmetric by necessity. These models have a forward center of gravity to achieve aerodynamic stability and to minimize pitch and yaw motion – a desired characteristic for models such as these.

Figure 13 shows two examples of launch packages. Fig. 13a is a saboted model for aerodynamic measurements of a lifting entry vehicle [30]. The launcher used for these tests was the 44 mm powder gun. Figure 13b shows an example of bore rider models used for measurements of transition induced by distributed roughness [32]. The 38.3 mm light gas gun was used to launch these models.

4.1.2 Sabot separation tank and vacuum system

The sabot separation tank (also referred to as the dump tank) consists of a vertical cylindrical tank, approximately 136 m^3, with transition extensions on either side that are in line with the test section and the light gas gun. Inside the dump tank and attached to the entrance of the test section extension is a large conical sabot stripper. This device has an adjustable aperture (1.9 to 15 cm dia.) that allows model passage, while the conical structure deflects and ultimately stops the sabot pieces. A thin Mylar diaphragm can be placed inside the stripper device to isolate the test section from the dump tank. The gun extension includes an entry hatch. At the top of the dump tank, extending above the building roof, is a port with a Mylar diaphragm to limit internal pressures to approximately atmospheric. The overall length of the assembly is 9.8 m. The volume, including the transition extensions, is approximately 144 m^3.

(a) (b)

Figure 13: Launch packages. (a) Model and sabot for aerodynamic measurements. Model is launched at an angle of attack. (b) Bore rider model for transition measurements.

The associated vacuum pumping system adjoining the dump tank is located below ground level. The system consists of a pair of rotary piston pumps and a Roots-type booster pump that are attached to the test section transition extension. In addition to these, another pair of rotary pumps is attached directly to the dump tank. A vacuum base pressure 2.4 Pa is attainable in the test section. Leak rates are less than 2.7 Pa per minute,

Figure 14: HFFAF test section showing shadowgraph stations.

despite the large numbers of windows and connections. Valves are pneumatically operated and electrically controlled from the control room under the downrange end of the test section.

4.1.3 Test section and shadowgraph stations

The test section, shown in Fig. 14, is 23 m long and has sixteen orthogonal shadowgraph stations spaced 1.5 m apart. The octagonal cross-section is approximately 1 m wide at the last downrange station. It has a slight taper, expanding in the uprange direction. The taper was designed to compensate for boundary-layer growth of the shock tunnel counterflow. The nominal width is 106 cm. The test section can operate from atmospheric pressure down to 2.4 Pa at ambient temperature. The test gases can be selected to simulate a variety of planetary atmospheres.

Each shadowgraph station includes four windows (top, bottom and both sides). The window diameters are 30.5 cm for stations 1 through 9, and 38.1 cm for stations 10 through 16. Window thicknesses are 25.4 mm and 32 mm, respectively. Each shadowgraph station is equipped with orthogonal-viewing parallel-light shadowgraph cameras and high-speed timers for recording the flight trajectories (position and angles as functions of time). Each view utilizes the following:

- Microsecond-duration spark light source mounted on the test section wall
- Pair of spherical mirrors mounted on the facility walls (for the horizontal view) or floor and ceiling (for the vertical view). The mirrors are the same diameter as the windows with focal lengths of approximately 1.8 m
- A 40 ns Kerr cell shutter at the focal point of the second mirror
- A light-excluding box for mounting a 20 cm x 25 cm sheet film holder

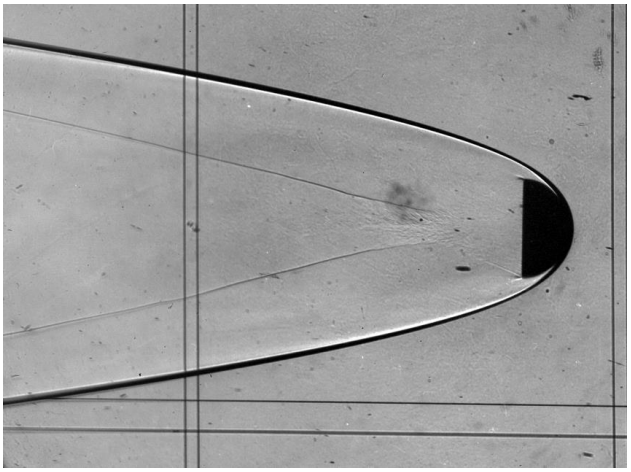

Figure 15: Shadowgraph image of a titanium hemisphere in flight in CO_2. V = 4.0 km/s, P = 20.3 Pa.

A photo-beam trigger system at each station activates the spark light source, triggers the Kerr cell shutters, and stops associated event timers to record the arrival time of the model at each station. The exact location of the model is read from each shadowgraph relative to a set of calibrated fiducial wires attached to the test section. This system provides up to 16 position/time measurements of the model's velocity, position, and orientation through the test section. Figure 15 shows an example shadowgraph image of a titanium hemisphere in free flight. The test gas was CO_2 at 20.3 Pa, and

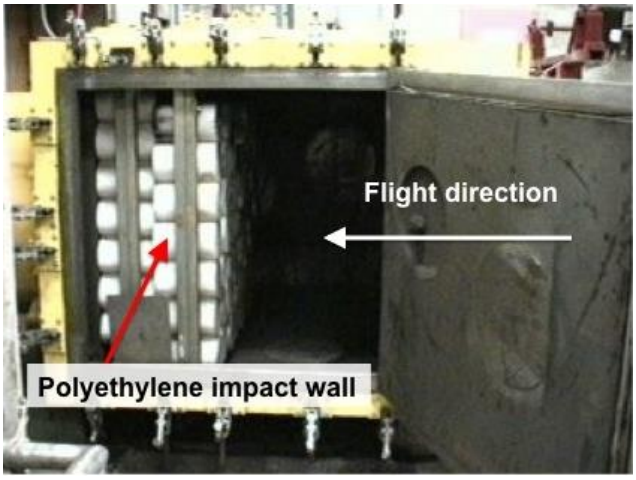

Figure 16: Test chamber and impact wall.

the velocity was 4.0 km/s (Mach 14.8) [33].

4.1.4 Impact/test chamber

The impact/test chamber is located between the test section and shock tunnel nozzle exit. It has two primary roles. When the facility is operated as a ballistic range alone, a 63.5 mm thick steel back stop and a 61 cm thick wall of polyethylene are installed at the nozzle exit to stop the aeroballistic models at the end of their flight (Fig. 16). Similarly, hypervelocity impact targets can be mounted in the chamber for this mode of operation. When the facility is operated as a shock tunnel alone, the chamber can be used as a free-jet test cabin for mounting large, highly instrumented models. For this mode of operation, the steel and polyethylene wall is removed, and diffuser panels are installed to smoothly redirect the shock tunnel flow into the test section. The impact/test chamber has several instrumentation feedthrough ports and four large access hatches (top, bottom, and both sides). Each hatch has two 38.1 cm. diameter window ports to provide optical access.

4.1.5 Shock tube and shock tunnel

As discussed in Section 2.1, the counterflow capability of the HFFAF has not been utilized since 1972, and the shock tunnel itself is on standby status. The shock tunnel operates in reflected mode and is comprised of a combustion driver, shock tube, and nozzle [28,79]. The combustion driver is 43.2 cm dia. and 21.3 m long. The driven tube is 30.5 cm dia. and 26 m long. The contoured nozzle has an exit diameter of 1 m and is 5.9 m long. It can operate at exit Mach numbers between 5 and 7. Throat inserts for the nozzle enable selection of area ratios from 95 to 271. The driver and driven tubes are separated by a flat, stainless-steel diaphragm with a thickness and score depth selected for rupture at a prescribed pressure. A thin Mylar diaphragm separates the driven tube and nozzle. The driver operates with cold He or combustion heated mixtures of air-He-H_2-O_2 or He-H_2-O_2. The driven tube is filled with the desired test gas (usually air). Selection of the driver gas composition, diaphragm burst pressure, and nozzle throat size enables flexibility in prescribing the total enthalpy and effective Mach number of the shock tunnel flow. The total enthalpies range from 1.8 MJ/kg to 7.5 MJ/kg [80]. The impact/test chamber, range test section, and dump tank are evacuated to a low pressure to ensure proper flow establishment.

4.2 Operational envelope

The operating envelope of the HFFAF, without conterflow, is shown in Fig. 17. The velocity range of the gun and the pressure range of the test section define the envelope's bounding box. Also shown in Fig. 17 is the Reynolds number range based on a model diameter of 2.54 cm. The regions where O_2 and N_2 dissociation and ionization become prevalent are indicated. Entry trajectories of several vehicles, plotted as altitude vs. velocity, are shown to indicate the overlap of the HFFAF envelope with these trajectories. The velocity and Reynolds number ranges of the HFFAF enable a wide array of aerodynamic and aerothermal phenomena to be evaluated in free flight. A variety of time-resolved optical instrumentation is available to characterize static and dynamic aerodynamic coefficients and model surface temperatures.

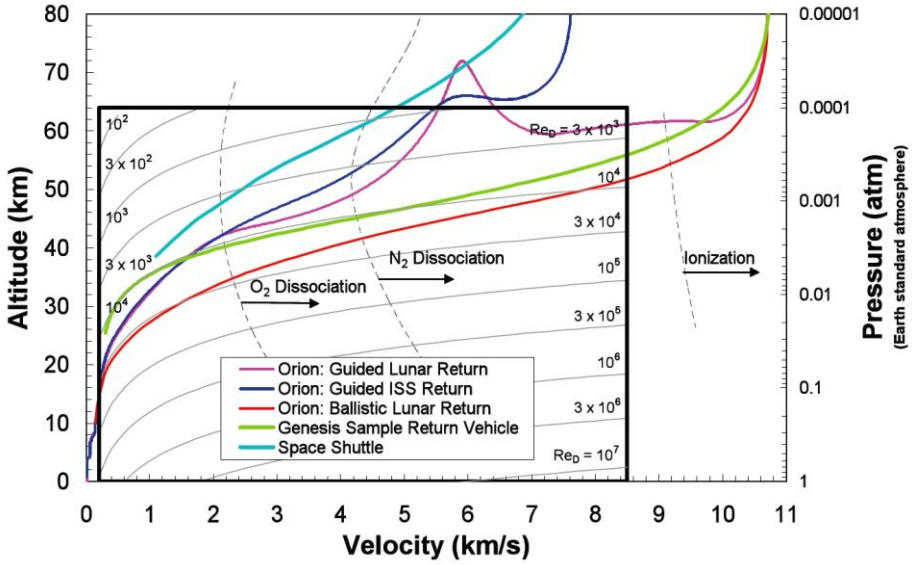

Figure 17: Testing envelope for HFFAF overlaid with selected Earth entry trajectories. Reynolds number contours are based on a 2.54 cm model in air.

CONCLUSION

The shock tube and ballistic range facilities at NASA Ames have supported a variety of test programs in the broad disciplines of aerodynamics and aerothermodynamics for almost fifty years. The facilities were built just before NASA's inception and during its brisk expansion in the 1960s. Agency initiatives for space exploration motivated the development of test facilities that could duplicate the extreme velocities and temperatures encountered in superorbital Earth atmospheric re-entry and entry into other planetary atmospheres. Efforts to realize these capabilities led to innovations in facility design, operation, and instrumentation. The legacy of that era continues with the agency's two premier high enthalpy impulse facilities: the HFFAF aeroballistic range and the EAST shock tube.

Current research programs utilizing the HFFAF concentrate on boundary layer transition due to surface roughness: augmented heat transfer arising from turbulent flow is a critical risk driver for the design of thermal protection materials and systems. The HFFAF provides a disturbance-free, quiescent environment that matches relevant high-enthalpy conditions of flight in Earth and other planetary atmospheres. Those characteristics, along with optimized test design methodologies, enable experiments for development and validation of physics-based models of transition. The EAST facility supports research in shock-layer radiation spectroscopy and transport. Radiative heat transfer becomes significant as vehicle entry speeds and sizes increase and therefore is also a critical risk driver for thermal protection design. The facility can replicate conditions behind shock waves at superorbital velocities in a variety of atmospheres. The facility is unique as it is the only known shock tube capable of generating shock velocities for Jovian entry.

REFERENCES

[1] Hartman, E.P., "Adventures in Research: A History of Ames Research Center, 1940-1965," SP-4302, NASA, p. 142, 1970.

[2] Seiff, A., James, C.S., Canning, T.N., and Boissevain, A.G., "The Ames Supersonic Free-Flight Wind Tunnel," RM A52A24, NACA, Apr. 1952.

[3] *Research Facilities Summary, Vol. I-Guns and Ranges*, NASA Ames Research Center, Moffett Field, CA, 1965.

[4] Sammonds, R.I., "Forces and Moments on an Apollo Model in Air at Mach Numbers to 35 and Effects of Changing Face and Corner Radii," TM X-1086, NASA, Apr. 1965.

[5] Intrieri, P.F., and Kirk. D.B., "High-Speed Aerodynamics of Several Blunt-Cone Configurations," *Journal of Spacecraft*, Vol. 24, No. 2, pp. 127-132, 1987.

[6] Strawa, A.W., Davy, W.C., and Kruse, R., "Measurements in the Wake of Blunt Aerobrake Models at 1.8 and 4.9 km/s," *Journal of Spacecraft and Rockets*, Vol. 30, No. 3, pp. 380-382, 1993.

[7] Intrieri, P.F., Kirk, D.B., Chapman, G.T., and Terry, J.E., "Ballistic Range Tests of Ablating and Nonablating Slender Cones," *AIAA Journal*, Vol. 8, No, 3, pp. 558-564, 1970.

[8] Bioletti, C., "An Atmosphere Entry Simulator," TM X-51119, NASA, Feb. 1959.

[9] Hamaker, F.M., "The Ames Atmosphere Entry Simulator and its Application to the Determination of Ablative Properties of Materials for Ballistic Missiles," TM X-394, NASA, Oct. 1960.

[10] Page, W.A., Canning, T.N., Craig, R.A., and Stephenson, J.D., "Measurements of Thermal Radiation of Air From the Stagnation Region of Blunt Bodies Traveling at Velocities up to 31,000 Feet per Second," TM X-508, NASA, Jun. 1961.

[11] Seiff, A., "Ames Hypervelocity Free-Flight Research," *Astronautics and Aerospace Engineering*, Vol. 1, No. 11, pp. 16-23, 1963.

[12] Page, W.A. and Arnold, J.O., "Shock-Layer Radiation of Blunt Bodies at Reentry Velocities," TR R-193, NASA, Apr. 1964.

[13] Borucki, W.J., "Spectrographic Observations of Polycarbonate, Polyethylene, and Polyformaldehyde in a Ballistic Range, an Arc Jet, and a Diffusion Flame," AIAA Paper No. 66-132, Jan. 1966.

[14] Canning, T.N., Seiff, A, and James, C.S., eds., "Ballistic Range Technology," AGARDograph No. 138, p. 186, AGARD, 1970.

[15] Intrieri, P.F., "Study of the Stability and Drag at Mach Numbers from 4.5 to 13.5 of a Conical Venus-Entry Body," TN D-2827, NASA, May 1965.

[16] Walters, E.E., "Free-Flight Measurements of Radiative Heating to the Front Face of the Apollo Reentry Capsule as a Function of Angle of Attack," TM X-851, NASA, Feb. 1964.

[17] Page, W.A., "A Survey of Thermal Radiation Studies of Ablating Bodies in the Ballistic Range," TN D-3741, NASA, Feb. 1967.

[18] Compton, D.L., and Cooper, D.M., "Measurements of Radiative Heating on Sharp Cones," *AIAA Journal*, Vol. 3, No. 1, pp. 107-114, 1965.

[19] Compton, D.L., "Measurements of Ultraviolet (575 Å – 1800 Å) Radiation from Nitrogen at Temperatures from 13,000 K to 16,000 K," AIAA Paper No. 66-422, 1966.

[20] Cooper, D.M., "High-Resolution Experimental Spectra and Theoretical Studies of Equilibrium Radiation from a Blunt Body Traveling at 37,000 Ft/Sec," AIAA Paper No. 66-104, 1966.

[21] Compton, D.L, and Cooper, D.M., "Free-Flight Measurements of Stagnation-Point Convective Heat Transfer at Velocities," TN D-2871, NASA, Jun. 1965.

[22] Boulgarides, J.D., Brown, W.S., and Richins, K.A., "Design of the Hypervelocity Free Flight Facility at NASA Ames Research Center," *The Performance of High Temperature Systems: Proceedings of the Third Conference*, Vol. 2, pp. 531-546, 1964.

[23] DeRose, C.E., "Trim Attitude, Lift and Drag of the Apollo Command Module with Offset Center-of-Gravity Positions at Mach Numbers to 29," TN D-5276, NASA, Jun. 1969.

[24] Miller, R.J., "Diverse Studies in the Reactivated NASA Ames Radiation Facility: From Shock Layer Spectroscopy to Thermal Protection System Impact," 45th Meeting of the Aeroballistic Range Association, Oct. 1994.

[25] Kirk, D.B., Intrieri, P.F., and Seiff, A. "Aerodynamic Behavior of the Viking Entry Vehicle: Ground Test and Flight Results, " *Journal of Spacecraft*, Vol. 15, No. 4, pp. 208-212, 1978.

[26] Intrieri, P.P., DeRose, C.E., and Kirk, D.B., "Flight Characteristics of Probes in the Atmospheres of Mars, Venus, and the Outer Planets," *Acta Astronautica*, Vol. 4, Nos. 7-8, pp. 789-799, 1977.

[27] Seiff, A., Reese, D.E., Sommer, S.C., Kirk, D.B., Whiting, E.E., and Niemann, H.B., "PAET, an Entry Probe Experiment in the Earth's Atmosphere," *Icarus*, Vol. 18, pp. 525-563.

[28] Bogdanoff, D.W., Zambrana, H.A., Cavolowsky, J.A., Newfield, M.E., Cornelison, C.J., and Miller, R.J., "Reactivation and Upgrade of the NASA Ames 16 Inch Shock Tunnel: Status Report," AIAA Paper 92-0327, Jan. 1992.

[29] Brown, J., Yates, L., Bogdanoff, D., Chapman, G., Loomis, M., and Tam, T., "Free-Flight Testing in Support of the Mars Science Laboratory Aerodynamics Database," *Journal of Spacecraft and Rockets*, Vol. 43, No. 2, pp. 293-302, 2006.

[30] Brown, J.D., Bogdanoff, D.W., Yates, L.A., and Chapman, G.T., "Free-Flight Dynamic Aero Data for a Lifting CEV Capsule," AIAA Paper No. 2008-1232, Jan. 2008.

[31] Reda, D.C., Wilder, M.C., Bogdanoff, D.W., and Olejniczak, J., "Aerothermodynamic Testing of Ablative Reentry Vehicle Nosetip Materials in Hypersonic Ballistic-Range Environments," AIAA Paper No. 2004-6829, Nov. 2004.

[32] Reda, D.C., Wilder, M.C., Bogdanoff, D.W., and Prabhu, D.K., "Transition Experiments on Blunt Bodies with Distributed Roughness in Hypersonic Free Flight, *Journal of Spacecraft and Rockets*, Vol. 45, No. 2, pp. 210-215, 2008.

[33] Reda, D.C, Wilder, M.C., and Prabhu, D.K., "Transition Experiments on Blunt Bodies with Isolated Roughness Elements in Hypersonic Free Flight," AIAA Paper No. 2010-1367, Jan. 2010.

[34] Cunningham, B.E. and Kraus, S., "A 1-Foot Hypervelocity Shock Tunnel in Which High-Enthalpy, Real-Gas Air Flows Can Be Generated with Flow Times of About 180 Milliseconds," TN D-1428, NASA, Oct. 1962.

[35] Compton, D.L., "Developments in Combustion Smoothness and Efficiency in a Large Shock-Tube Driver," TM X-56498, NASA, May 1965.

[36] Dannenberg, R.E., and Stewart, D.A., "Techniques for Improving the Opening of the Main Diaphragm in a Large Combustion Driver," TN D-2735, NASA, Mar. 1965.

[37] McKenzie, R.L. and Arnold, J.O., "Experimental and Theoretical Investigations of the Chemical Kinetics and Nonequilibrium CN Radiation Behind Shock Waves in CO_2–N_2 Mixtures," AIAA Paper No. 67-322, Apr. 1967.

[38] Arnold, J.O. and Nichols, R.W., "A Shock Tube Determination of the Electronic Transition Moment of the CN Red Band System," *Journal of Quantitative Spectroscopy and Radiative Transfer*, Vol. 12, No. 10, pp. 1435-1436, 1972.

[39] Arnold, J.O. and Nichols, R.W., "A Shock Tube Determination of the CN Ground State Dissociation Energy and the CN Violet Electronic Transition Moment," *Journal of Quantitative Spectroscopy and Radiative Transfer*, Vol. 13, No. 2, pp. 115-118, IN1-IN4, 119-133, 1973.

[40] Arnold, J.O. and Whiting, E.E., "Nonequilibrium Effects on Shock-Layer Radiometry During Earth Entry," *Journal of Quantitative Spectroscopy and Radiative Transfer*, Vol. 13, No. 9, pp. 861-870, 1973.

[41] Arnold, J.O, "A Shock Tube Determination of the Electronic Transition Moment of the C_2 (Swan) Bands," *Journal of Quantitative Spectroscopy and Radiative Transfer*, Vol. 8, No. 11, pp. 1781-94, 1968.

[42] Warren, W.R., Rodgers, D.A., and Harris, C.J., "The Development of an Electrically Heated Shock Driven Test Facility," 2nd Symposium on Hypervelocity Techniques, Univ. of Denver, Denver, CO, Mar. 1962.

[43] Grusczczynksi, J.S., and Warren, W.R., "Measurements of Hypervelocity Stagnation Point Heat Transfer in Simulated Planetary Atmospheres," Report No. R63SD29, General Electric Space Sciences Laboratory, Missiles and Space Division, Mar. 1963.

[44] Camm, J., "Escape Velocity Shock Tube With Arc Heated Driver," 2nd Symposium on Hypervelocity Techniques, Univ. of Denver, Denver, CO, Mar. 1962.

[45] Camm, J.C., and Rose, P.H., "Electric Arc Shock Tube," *Physics of Fluids*, No. 6, No. 5, pp. 663-667, 1963.

[46] Presley, L.L, Falkenthal, G.E., Naff, J.T., "One Megajoule Arc Discharge Shock Tube as a Chemical Kinetics Research Facility," TM X-56777, NASA, Jan. 1962.

[47] McClenahan, J.O., "Vacuum Ultraviolet Line Radiation Measurements of a Shock-heated Nitrogen Plasma," TN D-6920, NASA, Aug. 1972.

[48] Presley, L.L., Chackerian, Jr., C., and Watson, R., "The Dissociation Rate of Carbon Monoxide Between 7,000 K and 15,000 K," AIAA Paper No. 66-518, Jan. 1966.

[49] Omura, M. and Presley, L.L., "Electron Density Measurements Ahead of Shock Waves in Air," Vol. 7, No. 12, pp. 2363-2365, 1969.

[50] Reller, Jr., J.O., "Design and Performance of the Ames Electric Arc Shock Tunnel," TM X-2814, NASA, Jun. 1973.

[51] Sharma, S.P., Ruffin, S.M., Gillespie, W.D., and Meyer, S.A, "Vibrational Relaxation Measurements in an Expanding Flow Using Spontaneous Raman Scattering," *Journal of Thermophysics and Heat Transfer*, Vol. 7, No. 4, pp. 697-703, 1993.

[52] Sharma, S.P., Ruffin, S.M., Meyer, S.A., Gillespie, W.D., and Yates, L.A., "Density Measurements in an Expanding Flow Using Holographic Interferometry," *Journal of Thermophysics and Heat Transfer*, Vol. 7, No. 2, pp. 261-268, 1993.

[53] Bogdanoff, D. W., Park, C., and Mehta, U. B., "Experimental Demonstration of Magneto-Hydrodynamic (MHD) Acceleration—Facility and Conductivity Measurements," TM-2001-210922, July 2001, NASA.

[54] Park, C., and Bogdanoff, D.W., "Shock-Tube Measurement of Nitridation Coefficient of Solid Carbon," *Journal of Thermophysics and Heat Transfer*, Vol. 20, No. 3, 487-492, 2006.

[55] Bogdanoff, D.W., "Investigation of Electrical Conductivity of Shock Heated Air", appears in *Magnetohydrodynamics Accelerator Research into Advanced Hypersonics (MARIAH), Final Report*, by Baughman, J.A., Micheletti, D.A., Nelson, G L. and Simmons, G.A., NASA CR-97-206242, pp. A.2-1 to A.2-261, Oct. 1997.

[56] Bogdanoff, D.W., Wilson, G.J., and Sussman, M.A., "Experimental Demonstration of Use of N_2O to Increase Shock Tunnel Test Time," *AIAA Journal*, Vol. 35, No. 6, 1048-1056, 1997.

[57] Shirai, H., Park, C., "Experimental Studies of Radiative Base Heating of a Jovian Entry Model," AIAA Paper No. 79-0038, Jan. 1979.

[58] Jaffe, N.A., "Experimental Investigation of the Interaction Between Strong Shock Waves and Water Droplets," Aerotherm Report 75-156, Contract ONA001-74-C-OQ51, Aerotherm Division, Acurex Corporation, Jul. 1975.

[59] Dannenberg, R.E., and Silva, A.F., "Arc Driver Operation for Either Efficient Energy Transfer or High-Current Generation," TM X-62162, NASA, May 1972.

[60] Dannenberg, R.E., "A Conical Arc Driver for High-Energy Test Facilities," *AIAA Journal*, Vol. 10, No. 12, pp. 1692-1694, 1972.

[61] Dannenberg, R.E., and Slapnicar, P.I., "Development of Dynamic Discharge Arc Driver with Computer-Aided Circuit Simulation," *AIAA Journal*, Vol. 14, No. 9, pp. 1183-1188, 1976.

[62] Grinstead, J.H., Wilder, M.C., Olejniczak, J., Bogdanoff, D.W., Allen, G.A., Dang, K., and Forrest, M.J. "Shock-heated Air Radiation Measurements at Lunar Return Conditions," AIAA Paper No. 2008-1244, Jan. 2008.

[63] Cruden, B.A, Martinez, R., Grinstead, J.H., and Olejniczak, J., "Simultaneous Vacuum Ultraviolet through Near IR Absolute Radiation Measurement with Spatiotemporal Resolution in an Electric Arc Shock Tube," AIAA Paper No. 2009-4240, June 2009.

[64] Grinstead, J.H., Wright, M.J., Bogdanoff, D.W., and Allen, G.A., "Shock Radiation Measurements for Mars Aerocapture Radiative Heating Analysis," *Journal of Thermophysics and Heat Transfer*, Vol. 23, No. 2, pp. 249-255, 2009.

[65] Bose, D., Wright, M., Bogdanoff, D., Raiche, G.A., and Allen, G.A., "Modeling and Experimental Assessment of CN Radiation Behind a Strong Shock Wave", *Journal of Thermophysics and Heat Transfer*, Vol. 20, No. 2, pp. 220-230, 2006.

[66] Sharma, S.P., and Gillespie, W., "Nonequilibrium and Equilibrium Shock Front Radiation Measurements," *Journal of Thermophysics*, Vol. 5., No. 3, pp. 257-265, 1991.

[67] Sharma, S.P, and Whiting, E.E., "Modeling of Nonequilibrium Radiation Phenomena: An Assessment," *Journal of Thermophysics and Heat Transfer*, Vol. 10, No. 3, pp. 385-396, 1996.

[68] Meyer, S.A., Sharma, S.P., Bershader, D., Whiting, E.E., Exberger, R.J., and Gilmore, J.O., "Atomic Oxygen Line Shape Measurement at 130 nm with Raman-Shifted Laser," *AIAA Journal*, Vol. 34, No. 3, pp. 508-514, 1993.

[69] Bogdanoff, D.W., and Park, C., "Radiative Interaction Between Driver and Driven Gases in an Arc-Driven Shock Tube," *Shock Waves* Vol. 12, pp. 205-214, 2002.

[70] Holden, M.S., Wadhams, T.P., and MacLean, M., "Experimental Studies in the LENS Supersonic and Hypersonic Tunnels for Hypervelocity Vehicle Performance and Code Validation," AIAA Paper No. 2008-2505, May 2008.

[71] Tsai, C-Y., Chue, R., Nicholson, C., and Tyll, J., "Hypervelocity Capability of HyPulse Shock Tunnel for Radiative Heat Transfer Measurements at Lunar Reentries," AIAA Paper No. 2009-1516, Jan. 2009.

[72] Scott, M., Morgan, R., and Jacobs, P., "A New Single Stage Driver for the X2 Expansion Tube," AIAA Paper No. 2005-697, Jan. 2005.

[73] Morgan, R.G., "Development of X3, a Superorbital Expansion Tube," AIAA Paper No. 2000-558, Jan. 2000.

[74] Dannenberg, R.E., "Operating Parameters and Test Envelopes for the 1.22 MJ, 20/40 kV Energy Storage System and the 4-inch Arc-Driven Shock Tube," Report No. KDA 132, Arvin Calspan Contract C-87-17-01, Mar. 1990.

[75] Menard, W.A., "A Higher Performance Electric-Arc Driven Shock Tube," *AIAA Journal*, Vol. 9, No. 10, pp. 2096-2098, 1971.

[76] Sharma, S.P., and Park, C., "Operating Characteristics of a 60-cm and 10-cm Electric Arc Driven Shock Tube, Part I: The Driver; Part II: The Driven Section", *Journal of Thermophysics and Heat Transfer*, Vol. 4, pp. 259-265; pp. 266-272, 1990.

[77] Mirels, H., and Braun, W.H., "Nonuniformities in Shock-Tube Flow Due to Unsteady-Boundary-Layer Action," TN 4021, NACA, May 1957.

[78] Canning, T.N., Seiff, A, and James, C.S., eds., "Ballistic Range Technology," AGARDograph No. 138, AGARD, p. 11, 1970.

[79] ibid., p. 173.

[80] ibid., p. 186.